Z. Phys. B – Condensed Matter 65, 381–395 (1987)

Condensed
Zeitschrift für Physik B Matter

Classical and Quantum Chaos for a Kicked Top

F. Haake, M. Kuś*, and R. Scharf
Fachbereich Physik, Universität-Gesamthochschule Essen, Federal Republic of Germany

Received June 5, 1986

We discuss a top undergoing constant precession around a magnetic field and suffering a periodic sequence of impulsive nonlinear kicks. The squared angular momentum being a constant of the motion the quantum dynamics takes place in a finite dimensional Hilbert space. We find a distinction between regular and irregular behavior for times exceeding the quantum mechanical quasiperiod at which classical behavior, whether chaotic or regular, has died out in quantum means. The degree of level repulsion depends on whether or not the top is endowed with a generalized time reversal invariance.

1. Introduction

The quantum treatment of systems capable of chaotic motion in the classical limit is interesting for several reasons. First, there is the desire to see how the classical distinguishability between regular and chaotic motion gradually arises as the system is turned more and more classical by changing a suitable parameter. By a controlled increase of quantum mechanical time scales such as wave packet spreading times or inverse level spacings, for instance, one would like to study the growth of the life time of effectively chaotic evolution of suitable observables.

Perhaps an even greater incentive for quantum mechanical investigations lies in the question whether quantum chaos can be more than a mere transient mimicry of classical chaos. If so, we need intrinsically quantum mechanical criteria to distinguish regular an irregular behavior; the relation of such quantum criteria to the traditional ones for classical chaos would have to be clarified.

We shall here present a model system ideally suited to a study of the problems mentioned, a three dimensional angular momentum **J** moving such that its square is conserved. Quantum mechanically, we can identify the operator $\mathbf{J}^2$ with its eigenvalue $j(j+1)$ and thus have a Hilbert space with the finite dimensionality $(2j+1)$. As the quantum number j is increased the quantum behavior approaches the classical one. We choose the Hamiltonian so as to allow for classically chaotic behavior as $j \to \infty$. The simplest such Hamiltonian accounts for a precession of **J** around a constant a constant external magnetic field as well as for a periodic train of impulsive nonlinear kicks. A stroboscopic description is then indicated, the basis ingredient being the unitary operator U which transports the state vector from kick to kick.

The perhaps most important feature of our model is the finite dimensionality of its Hilbert space. Previous studies of quantum billiards [1] and the kicked rotator [2] had to confront the intricacies of an infinite number of dimensions. As Casati et al. have recently emphasized [3], an equivalence of U to certain ensembles of random matrices is much more difficult to establish for an infinite then a finite number N of dimensions. Of course, actual calculations (of, say, eigenvalues or time dependent expectation values) for systems with infinite N always have to truncate the Hilbert space to some manageable finite size. There is the danger, then, of introducing a new or destroying some hidden symmetry. In fact, Izrailev [4, 5] has recently pointed out that the eigenvalues of U for the kicked rotator can be given drastically different statistical properties by different truncation schemes.

Our model can be endowed with various symmetries. Among those are discrete rotations and nonconventional time reversals. The classical analysis is greatly facilitated by these symmetries and yields a surprising wealth of analytic results for fixed points, periodic orbits, and the stability scenario. In the quantum case symmetries play an even greater role. Two variants of the model, one with and the other without time reversal invariance, belong to different universality classes with respect to the statistics of the eigenvalues of U.

* Permanent address: Institute of Theoretical Physics, Warsaw University, Hoza 69, PL-00-681 Warsaw, Poland

Due to the discreteness of the spectrum of our U all quantum expectation values behave quasiperiodically in time [6], the quasiperiod being of the order j (in units of the kick period). Since classical chaos can become manifest on a time scale $\sim \ln j$ (the time needed to amplify the minimum quantum uncertainty $\sim 1/\sqrt{j}$ of the orientation of $\mathbf{J}$ to a solid angle of order unity) rather modest values of j suffice to realize classical chaos as a transient and to observe the subsequent takeover of quasiperiodicity. It is most fascinating, however, to see quasiperiodicity on the time scale j to arise in two qualitatively different varieties.

Rather regularly shaped collapses and revivals of quantum means alternate with a (quasi)period $\sim j$ when all external parameters and the initial state are set such that the classical limit would yield regular trajectories. However, under the conditions of classical chaos quantum means display a seemingly erratic behavior even on the time scale j; recurrences to a close neighborhood of the initial means do occur on that scale but have no tendency towards constant temporal separation.

Much insight can be gained from a spectral synthesis of quantum means based on the eigenvalues and eigenvectors of U. We find a rather small number of modes to be excited under the conditions of classically regular motion while classical chaos always corresponds to a large fraction of all modes in action. Regularly alternating collapses and revivals are thus revealed as a quantum beat phenomenon while the erratic variety of quasiperiodicity corresponds to broad-band excitation.

Previous analyses of level statistics have mostly focused on autonomous Hamiltonian systems [1, 7, 8, 9]. In our case of a kicked system we have to discuss the eigenphases of the unitary operator U. Of special interest is the relative frequency of a spacing S of two neighboring ones among the $2j+1$ eigenphases. We expect and numerically confirm a Poisson distribution of S to correspond to classically regular motion [10]. To investigate the level statistics corresponding to classical chaos we extend previous theories for autonomous systems to kicked ones. We also discuss the influence of time reversal invariance on the level spacing distribution. On the basis of this discussion we predict linear level repulsion, $P(S) \sim S$ for $S \to 0$, for the variant of our model for which we have identified a time reversal invariance. After breaking that invariance by a slight modification of the dynamics and assuming that there is no unidentified hidden antiunitary symmetry we should expect quadratic level repulsion, $P(S) \sim S^2$ for $S \to 0$. These theoretical predictions are nicely confirmed by our numerical results.

Preliminary results of our work were reported in [11]. We should also refer the reader to independent work on a similar model by Frahm and Mikeska [12].

2. The Quantum Top

We imagine as system characterized by an angular momentum vector $\hbar \mathbf{J} = \hbar(J_x, J_y, J_z)$, $[J_i, J_j] = i\varepsilon_{ijk} J_k$. The dynamics of $\mathbf{J}$ is governed by the Hamiltonian

$$H(t) = +(\hbar p/\tau) J_y + (\hbar k/2j) J_z^2 \sum_{n=-\infty}^{+\infty} \delta(t - n\tau). \tag{2.1}$$

The first term in $H(t)$ describes a precession around the y axis with angular frequency p/τ while the second term accounts for a periodic sequence of kicks at a temporal distance τ. Each kick can be interpreted as an impulsive rotation around the z axis by an angle proportional to J_z, the proportionality factor involving a dimensionless coupling constant k/j.

The following investigation is most conveniently formulated with the help of the unitary time evolution operator

$$U = \mathrm{e}^{-\mathrm{i}(k/2j)J_z^2} \mathrm{e}^{-\mathrm{i}pJ_y} \tag{2.2}$$

which subjects the wave function to a precession around the y axis by an angle p and the subsequent kick. The powers U^n describe the time evolution on the sequence of discrete times $n\tau$, $n = 0, 1, 2, \ldots$. In the Schrödinger picture, an initial state $|0\rangle$ developes, within n units of time, into the state $|n\rangle = U^n |0\rangle$. In the Heisenberg picture the discrete time evolution generates a sequence of operators $J_{in} = U^{+n} J_i U^n$. The corresponding Heisenberg equations take the form of nonlinear operator recursion relations,

$$\begin{aligned} J_x' &= \tfrac{1}{2}(J_x \cos p + J_z \sin p + \mathrm{i} J_y) \mathrm{e}^{\mathrm{i}\frac{k}{j}(J_z \cos p - J_x \sin p + \frac{1}{2})} \\ &\quad + \text{h.c.} \\ J_y' &= \tfrac{1}{2i}(J_x \cos p + J_z \sin p + \mathrm{i} J_y) \mathrm{e}^{\mathrm{i}\frac{k}{j}(J_z \cos p - J_x \sin p + \frac{1}{2})} \\ &\quad + \text{h.c.} \\ J_z' &= J_z \cos p - J_x \sin p. \end{aligned} \tag{2.3}$$

We shall devote special attention to the precession angle $p = \pi/2$ for which the recursion relations (2.3) simplify considerably.

Evidently, the squared angular momentum is a conserved quantity,

$$\begin{aligned} [\mathbf{J}^2, H(t)] &= 0, \\ [\mathbf{J}^2, U] &= 0. \end{aligned} \tag{2.4}$$

We can therefore restrict our discussion to the $(2j+1)$ dimensional Hilbert space spanned by the eigenvectors of J_z and $\mathbf{J}^2$,

$$\mathbf{J}^2 |jm\rangle = j(j+1)|jm\rangle$$
$$J_z |jm\rangle = m|jm\rangle. \tag{2.5}$$

Initial states of special importance for our eventual goal of comparing quantum and classical dynamics are the directed angular momentum states [13, 14]

$$|\theta, \phi\rangle = (1+\gamma\gamma^*)^{-j} e^{\gamma J_-} |j,j\rangle \equiv |\gamma\rangle,$$
$$\gamma = e^{i\phi} \tan\frac{\theta}{2}, \tag{2.6}$$
$$J_- = J_x - iJ_y.$$

These states align, with minimum uncertainty, the vector $\mathbf{J}$ along a direction characterized by a polar angle θ and an azimutal angle ϕ,

$$\langle\theta\phi|J_z|\theta\phi\rangle = j\cos\theta$$
$$\langle\theta\phi|J_x \pm iJ_y|\theta\phi\rangle = je^{\pm i\phi}\sin\theta. \tag{2.7}$$

One such state is the basis vector $|jm\rangle$ with $m=j$. All other directed angular momentum states can be generated from the state $|jj\rangle$ by the unitary rotation operator

$$R(\theta,\phi) = \exp\{i\theta(J_x\sin\phi - J_y\cos\phi)\}. \tag{2.8}$$

The relative variance of $\mathbf{J}$ in a state $|\theta\phi\rangle$,

$$(1/j^2)\{\langle\theta\phi|\mathbf{J}^2|\theta\phi\rangle - \langle\theta\phi|\mathbf{J}|\theta\phi\rangle^2\} = 1/j, \tag{2.9}$$

is the minimum one allowed by the angular momentum commutation relations, it evidently shrinks to zero as the quantum number j grows towards infinity, i.e. in the classical limit.

We shall characterize the quantum dynamics of our top by the means and the variances of the operators J_{in} with respect to the "coherent" initial states $|\theta\phi\rangle$.

Experimental realizations of the dynamics (2.2, 3) might be possible in different fields. One example are small magnetized solids; crystal anisotropies allowing for an easy plane of magnetization can be represented by a time independent term $\sim J_z^2$ in the Hamiltonian; a temporally periodic sequence of short magnetic field pulses oriented along the y axis would have to be imposed to generate dynamics described by (2.2, 3). Experiments performed by Waldner et al. [15] are of precisely this type but refer to truely macroscopic magnetizations (j effectively infinite) and thus pertain to the classical limit. It would be extremely interesting to redo this kind of investigation with small clusters of particles.

Another type of experiment is conceivable using Josephson junctions with a capacitance in parallel. In a crude approximation, the Cooper pairs of the two superconductors joined can be described so as to be created and annihilated by Bose operators a_i^+, a_i with $i=1, 2$. The net charge on the junction can then be represented by an operator $S_z = (a_2^+ a_2 - a_1^+ a_1)/2$ while operators $S_x = (a_2^+ a_1 + a_1^+ a_2)/2$, $S_y = (a_2^+ a_1 - a_1^+ a_2)/2i$ describe the tunneling of Cooper pairs through the junction. By a suitable temporal modulation of the capacitance an effective Hamiltonian of the form (2.1) might then be realized [16] since the operators S_i have angular momentum commutation relations among themselves.

3. Regular and Chaotic Classical Motion on the Sphere

Before facing the intricacies of the quantum dynamics it is well to study the classical behavior arising for $j\to\infty$. In order to perform the limit we may introduce the rescaled quantities $\mathbf{X}=\mathbf{J}/j$ which fulfill the commutation relations $[X_i, X_k] = (1/j)\,\varepsilon_{ikl}\,X_l$. As $j\to\infty$ the X_i obviously become c-number variables which lie on the unit sphere. Their stroboscopic time evolution is described by a map which follows from the quantum recursion relations (2.3) with $j\to\infty$,

$$\left.\begin{matrix} X' \\ Y \end{matrix}\right\} = \begin{cases} \mathrm{Re} \\ \mathrm{Im} \end{cases} (X\cos p + Z\sin p + iY)\, e^{ik(Z\cos p - X\sin p)}$$
$$Z' = -X\sin p + Z\cos p. \tag{3.1}$$

We shall sometimes use the shorthand $\mathbf{X}' = F(\mathbf{X})$ for the map (3.2) and correspondingly write $\mathbf{X} = F^{-1}(\mathbf{X}')$ for its inverse,

$$X = (X'\cos kZ' + Y'\sin kZ')\cos p - Z'\sin p$$
$$Y = -X'\sin kZ' + Y'\cos kZ' \tag{3.2}$$
$$Z = (X'\cos kZ' + Y'\sin kZ')\sin p + Z'\cos p.$$

The conservation law (2.4) entails $\mathbf{X}^2 = 1$ and thus makes our classical map a two dimensional one. We could obviously rewrite it as two recursion relations for a polar and an azimutal angle according to

$$X = \sin\theta\cos\phi,\ Y = \sin\theta\sin\phi,\ Z = \cos\theta. \tag{3.3}$$

These angles are the classical counterparts of the angles characterizing the orientation of the coherent states (2.6).

Two further symmetries of our map are of great help for the further analysis. Consider first the operations $\mathbf{X}' = T(\mathbf{X})$ and $\mathbf{X}' = \tilde{T}\mathbf{X}$ defined by

$$T\begin{pmatrix} X \\ Y \\ Z \end{pmatrix} = \begin{pmatrix} -X\cos p - Z\sin p \\ Y \\ -X\sin p + Z\cos p \end{pmatrix} \tag{3.4}$$

and

$$\tilde{T}\begin{pmatrix} X \\ Y \\ Z \end{pmatrix} = \begin{pmatrix} X\cos p + Z\sin p \\ Y \\ X\sin p - Z\cos p \end{pmatrix} \tag{3.5}$$

They are both involutions,

$$T^2=\tilde{T}^2=1, \tag{3.6}$$

and have the determinants

$$\det T=\det\tilde{T}=-1. \tag{3.7}$$

It is easily verified that they both yield time reversal operations for our map F in the sense

$$TFT=\tilde{T}F\tilde{T}=F^{-1}. \tag{3.8}$$

Our top thus has (doubly reversible dynamics [17]. It is worth noticing, however, that neither T nor $\tilde{T}$ is the conventional time reversal $\mathbf{J}\to-\mathbf{J}$, the latter cannot yield an invariance since our dynamics involves precession around a magnetic field.

It follows immediately that the images under T and $\tilde{T}$ of n-periodic orbits of F, $F^n(\mathbf{X})=\mathbf{X}$, are n-periodic orbits of F as well. It may, of course, happen that such an orbit coincides with this own image.

It is another important consequence of the time reversal invariance of F that we can decompose F into a product of two involutions

$$F=T(TF) \tag{3.9}$$

(and similarly with $\tilde{T}$) since $(TF)^2=(FT)^2=1$, $(\tilde{T}F)^2=(F\tilde{T})^2=1$. Such decompositions greatly facilitate the search for periodic orbits. As a first step towards their employment we introduce the "symmetry lines" for the various involutions, i.e. the set of all points $\mathbf{X}$ obeying

$$I(\mathbf{X})=\mathbf{X} \quad \text{and} \quad \mathbf{X}^2=1 \tag{3.10}$$

for $I=T, \tilde{T}, FT, TF, \ldots$. For instance, the symmetry lines of T and $\tilde{T}$ (to be referred to as T line etc.) are the great circles on the unit sphere defined by $X\sin p-(\cos p-1)Z=0$ and $X\sin p-(\cos p+1)Z=0$, respectively. The other symmetry lines tend to have more complicated shapes for general values of the precession angle p. For $p=\pi/2$, however, we still have great circles with $Z=0$ for $F\tilde{T}$ and with $X=0$ for $\tilde{T}F$, while the intersections of the unit sphere with $X(\cos kZ+1)+Y\sin kZ=0$ and $Z(\cos kX+1)+Y\sin kZ=0$ are the symmetry lines for FT and TF, respectively.

As an illustration of the use of time reversal invariance we propose to consider a point $\mathbf{X}$ on, say, the T line. If the n-th iterate $F^n(\mathbf{X})$ also lies on the T line or on the symmetry line of either TF of FT, that point is periodic with period $2n$, $2n+1$, and $(2n-1)$, respectively [17, 18]. We may thus search for, say, period-$2n$ solutions of F by studying F^n (instead of F^{2n}).

It is also easily shown that any periodic orbit of F with even (odd) period which is invariant under any of the involutions in question has an even (odd) number of points on the corresponding symmetry line.

Beyond being symmetric under the time reversals T and $\tilde{T}$ our map F is invariant under rotations around the precession axis by π,

$$R_yF=FR_y \quad \text{with} \quad R_y\begin{pmatrix}X\\Y\\Z\end{pmatrix}=\begin{pmatrix}-X\\Y\\-Z\end{pmatrix}. \tag{3.11}$$

Actually, the three symmetries T, $\tilde{T}$, and R_y are not independent since $R_yT=TR_y=\tilde{T}$, $\tilde{T}T=T\tilde{T}=R_y$. It follows that the R_y image of every n-cycle of F is an n-cycle of F, too.

Specializing, for the remainder of this section, to $p=\pi/2$ we have the further symmetry

$$FR_x=R_xFR_y \quad \text{with} \quad R_x\begin{pmatrix}X\\Y\\Z\end{pmatrix}=\begin{pmatrix}X\\-Y\\-Z\end{pmatrix}. \tag{3.12}$$

This implies that the iterated map F^2 is invariant under rotations around the x-axis by π,

$$R_xF^2=F^2R_x. \tag{3.13}$$

The most important consequence of (3.12, 13) is that every $(2n+1)$-cycle of F together with its R_y image is mapped, by R_x, into a $(4n+2)$-cycle of F, provided the $(2n+1)$-cycle in question is not symmetric under R_y.

Let us now look at the fixed points of F. Evidently, the poles

$$X=Z=0, \qquad Y=\pm1 \tag{3.14}$$

with respect to the precession axis are invariant under F for any value of the kick strength k. Further, nontrivial fixed points appear for sufficiently large $|k|$. They are determined by

$$Z=-X, \qquad Y=X\cot\frac{kX}{2}, \qquad f(X)=0$$

$$\text{with } f(X)=\sin^2(kX/2)\{1+\sin^2(kX/2)\}^{-1}-X^2$$

and thus come in pairs, too. They all lie on the T line. One member of each pair can be generated from the other by R_y. It therefore suffices to consider only fixed points with $X>0$. We may also confine ourselves to positive kick strengths since a change of sign in k is equivalent to changing the sign of Y for the fixed points.

A graphical analysis of (3.15) easily reveals that (*i*) the first nontrivial solution emerges for $k_0=2$ and (*ii*) additional pairs of nontrivial fixed points appear when k crosses the thresholds k_j, $j=1, 2, 3, \ldots$ deter-

mined by $f(X)=0, f'(X)=0$, and $\mathbf{X}^2=1$. These thresholds are easily found numerically.

To discuss stability we need to linearize the map F around the various fixed points. Due to angular momentum conservation, $\mathbf{X}^2=1$, one of the three eigenvalues of the linearized map is, for all fixed points, equal to unity and thus irrelevant for stability. The other two eigenvalues are equal to unity in modulus provided the X and Y coordinates of the fixed point in question obey

$$|kY+\cos kX-1|<2. \tag{3.16}$$

The trivial fixed points are thus stable for $k<2$. The nontrivial fixed point emerging for $k\geqslant k_0=2$ is stable for $k_0\leqslant k\leqslant k_0'=\sqrt{2}\pi$. Of the pair of fixed points appearing at $k>k_j$ the member with the smaller value of X is always unstable while the other member is stable for

$$k_j\leqslant k\leqslant k_j'=(2j+1)\sqrt{2}\pi, j=1,2,\ldots. \tag{3.17}$$

When the kick strength crosses one of the thresholds k_j' the fixed point which looses its stability bifurcates into the period-2 solution

$$\begin{aligned} &X_1=X_2=-Z_1=-Z_2=(2j+1)\pi/k \\ &Y_1=-Y_2=\{1-2(2j+1)^2\pi^2/k^2\}^{1/2}. \end{aligned} \tag{3.18}$$

Like the fixed point it originates from it lies on the symmetry line of T. Once again linearizing we find the stability range

$$k_j'<k<k_j''=\sqrt{k_j'^2+4}. \tag{3.19}$$

As we increase k beyond k_j'' we generate a period-4 orbit and, for yet higher k, a whole cascade of period doublings with orbits symmetric under T.

Similar structures are revealed by investigating the $\tilde{T}$ line which is the R_y image of the T line. There are period-2 solutions

$$X_1=Z_1=-X_2=-Z_2, \qquad Y_2=Y_1=-X_1\cot\frac{kX_1}{2} \tag{3.20}$$

with X_1 again a root of the function $f(X)$ defined in (3.15). It is, of course, due to the invariance (3.12) that the operation R_x rotates each fixed point (3.15) and its R_y image to the location of the period-2 cycle and vice versa. The first of these cycles bifurcates from the "south" pole with respect to the precession axis when $k=k_0=2$ and pairs of cycles emerge at the thresholds k_j with $j=1, 2,\ldots$. Each cycle shares its stability properties with the corresponding pair of fixed points. The cycle loosing stability at k_j bifurcates into the period-4 orbit

$$\begin{aligned} &X_1=Z_1=-X_2=-Z_2=X_3=Z_3=-X_4=-Z_4 \\ &\quad=(2j+1)\pi/k, \\ &Y_1=-Y_2=Y_3=-Y_4=\{1-2(2j+1)^2\pi^2/k^2\}^{1/2} \end{aligned} \tag{3.21}$$

which remains stable in the range (3.19). Evidently, it lies on the $\tilde{T}$ line and can be found by rotating the 2-cycle (3.18) together with its R_y image around the X-axis by π.

Due to the high symmetry of our model we can easily find further periodic orbits. Of importance for us will be the period-4 cycle

$$\mathbf{X}_1=-\mathbf{X}_3=\begin{pmatrix}0\\0\\1\end{pmatrix}, \qquad \mathbf{X}_2=-\mathbf{X}_4=\begin{pmatrix}1\\0\\0\end{pmatrix}. \tag{3.22}$$

Note that this orbit lies on the "equator" with respect to the precession axis with $\mathbf{X}_1$ and $\mathbf{X}_3$ on the $\tilde{T}F$ line and $\mathbf{X}_2$ and $\mathbf{X}_4$ on the $F\tilde{T}$ line. It exists for arbitrary values of the kick strength but is stable only for $(2\cos k+k\sin k)^2<4$.

Another sequence of 4-cycles

$$\begin{aligned} &X_1=Z_1=X_2=-Z_2=-X_3=-Z_3=-X_4=Z_4, \\ &Y_1=-Y_2=Y_3=-Y_4=X_1\tan\frac{kX_1}{2}, \\ &\cos^2(kX_1/2)/\{1+\cos^2(kX_1/2)\}-X_1^2=0, \end{aligned} \tag{3.23}$$

has $\mathbf{X}_1$ and $\mathbf{X}_3$ on the $\tilde{T}$ line and $\mathbf{X}_2$ and $\mathbf{X}_4$ on the T line. It is thus symmetric under both T and $\tilde{T}$. The stability scenario is similar to the one of the fixed points (3.15).

There are interesting 3-cycles

$$\begin{aligned} &X_1=Z_1=-Z_2=-X_3, X_2=Z_3=0, \\ &Y_1=-X_1\cot kX_1, Y_2=Y_3=-X_1/\sin kX_1, \\ &\sin^2 kX_1/\{1+\sin^2 kX_1\}-X_1^2=0 \end{aligned} \tag{3.24}$$

and

$$\begin{aligned} &Z_1=Z_2=-X_1=-X_3 \\ &Z_3=-X_2, Y_2=Y_3 \\ &X_2=-X_1\cos kX_1+Y_1\sin kX_1 \\ &Y_2=X_1\sin kX_1+Y_1\cos kX_1 \end{aligned} \tag{3.25}$$

where X_1, Y_1 are given by solutions of the equations:

$$\begin{aligned} &X_1\left[\operatorname{ctg}\left(\frac{k}{2}X_1\cos kX_1\right)-\sin kX_1\right]+Y_1\cos kX_1=0 \\ &2X_1^2+Y_1^2=1. \end{aligned}$$

The 3-cycles (3.24) are symmetric under $\tilde{T}$ while the ones given in (3.25) are T invariant. Both types arise in pairs with each member the image of the other

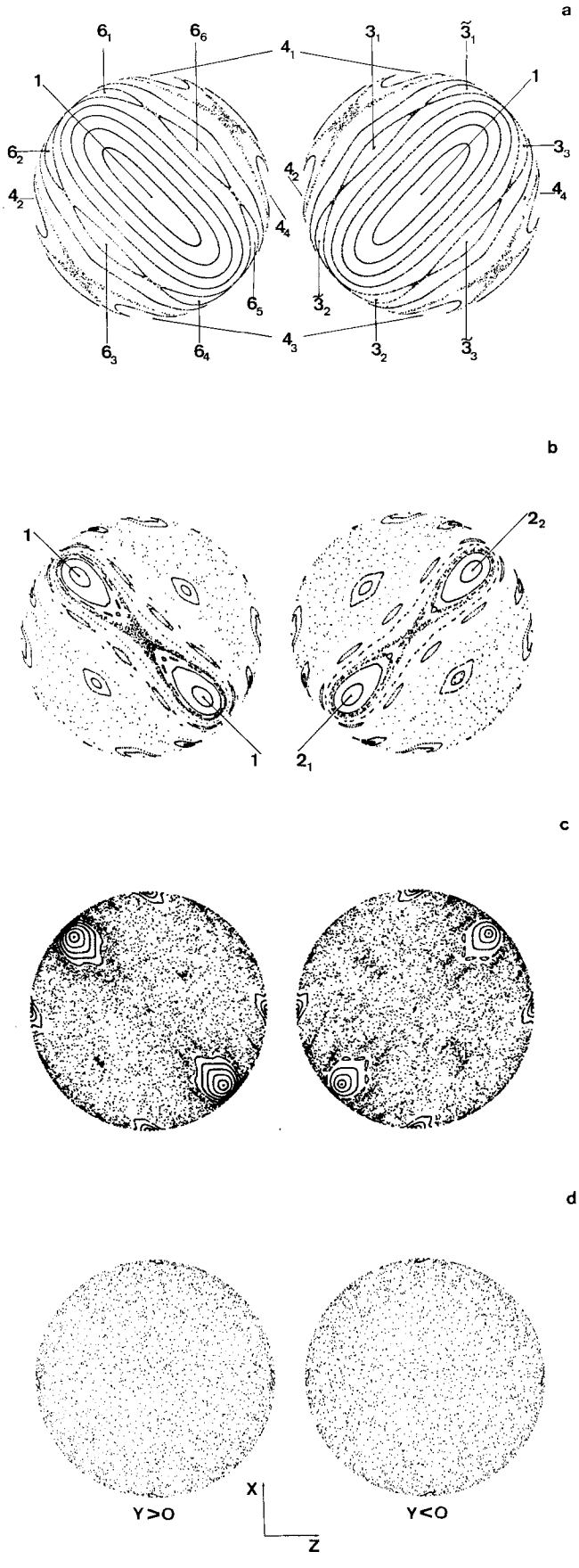

under R_y. Due to (3.12) each such pair yields, upon rotation around the X-axis by π, a 6-cycle.

All of the stable fixed points and periodic orbits discussed in the above show up in Fig. 1 which portraits trajectories generated by the map F for $p=\pi/2$ and various values of the kick strength k. Figure 1a pertains to $k=2$, a case where the fixed points at the poles (3.14) are still marginally stable. Most of the sphere is then covered by the stability islands around these fixed points, around the 4-cycle (3.22), and a pair of 3-cycles (3.25) together with their R_x image; narrow chaotic bands are visible near the first of the 4-cycles (3.23) and also near a pair of 3-cycles (3.24) and their R_x image which are unstable at $k=2$.

The somewhat richer structure arising for $k=2.5$ is displayed in Fig. 1b. The precession poles have now become hyperbolic fixed points and thus have chaotic trajectories in their neighborhoods. A pair of stable fixed points (3.15) in the "northern" hemisphere ($Y>0$) and, as their R_x image, the period-2 orbit (3.20) in the "southern" hemisphere now have prominent stability islands, as does the 4-cycle (3.22). Quite conspicuous is a pair of 3-cycles (3.24) in the southern hemisphere and their northern correspondant by R_x, a 6-cycle. A southern pair of 5-cycles, one the R_y image of the other, and, at R_x symmetric locations, a northern 10-cycle are also discernible. Apart from further but much smaller islands of stability the rest of the sphere accommodates chaos.

Chaos has become much more predominant for $k=3$, as is shown in Fig. 1c. It is only the stability islands of the northern pair of fixed points (3.15) and the corresponding southern 2-cycle (3.20) and of the equatorial 4-cycle (3.22) that are easily detected numerically. Note that the points (3.15, 20) have approached the equator quite closely. For $k=k_0'=\pi\sqrt{2}$ they will have arrived at $Y=0$ and go unstable.

At $k=6$, the case described by Fig. 1d, only tiny islands of stability around the equatorial 4-cycle (3.22) remain visible. There may be other unresolved stability islands but clearly, chaos has expanded to near-global dominance.

We should emphasize once again that there are whole generations of solutions of the equations determining fixed points and other periodic orbits. Therefore, regular structures keep reappearing as k is in-

Fig. 1a–d. Classical motion on the unit sphere. The left and right columns depict trajectories on the northern ($Y\geqslant 0$) and the southern ($Y\leqslant 0$) hemisphere, respectively. Fixed points are labeled by 1, points on n-cycles by n_i or $\tilde{n}_i$. **a**: $p=\frac{\pi}{2}$, $k=2$; **b**: $p=\frac{\pi}{2}$, $k=2.5$; **c**: $p=\frac{\pi}{2}$, $k=3$; **d**: $p=\frac{\pi}{2}$, $k=6$

creased. However, the corresponding stability islands on the sphere as well as the stability windows on the k axis shrink as we go through the sequence of generations.

4. Symmetries of the Quantum Top

There are quantum counterparts to all of the symmetries of the classical top. Their importance for the analysis of the quantum dynamics is even greater than in the classical case. For the sake of convenience of presentation we shall formulate them for integer values of j only. In that case the rotation operators

$$R_v = e^{\pm i\pi J_v} \tag{4.1}$$

are effectively hermitian.

Of special interest are the eigenvalues and eigenvectors of the unitary time evolution operator (2.2),

$$U|\phi\rangle = e^{i\phi}|\phi\rangle, \tag{4.2}$$

which we must construct, for a given j, as superpositions of the $2j+1$ states defined in (2.5). By observing the invariance of U under rotations around the y-axis by π,

$$[U, R_y] = 0, \tag{4.3}$$

the analogue of the classical symmetry (3.11), we find that the $2j+1$ eigenstates of U fall, for j even, into a group of $(j+1)$ states $|\phi_+\rangle$ which are even under R_y and another one of j states $|\phi_-\rangle$ which are odd,

$$U|\phi_\pm\rangle = e^{i\phi_\pm}|\phi_\pm\rangle, \quad R_y|\phi_\pm\rangle = \pm|\phi_\pm\rangle. \tag{4.4}$$

By again specializing to $p=\pi/2$ we obtain the quantum version of (3.12),

$$UR_x = R_x U R_y, \tag{4.5}$$

which entails the invariance of U^2 under R_x. With respect to the vectors $|\phi_\pm\rangle$ the identity (4.4) means

$$UR_x|\phi_\pm\rangle = \pm e^{i\phi_\pm} R_x|\phi_\pm\rangle. \tag{4.6}$$

An eigenphase ϕ_- is thus accompanied by $\phi_- + \pi$ as another one, both pertaining to states odd under R_y. On the other hand, the even states $|\phi_+\rangle$ and $P_x|\phi_+\rangle$ are either linearly dependent, or else the eigenvalue ϕ_+ is doubly degenerate.

For any value of the precession angle p we have, like in the classical case, two generalized time reversal symmetries which are represented by antiunitary operators. To construct them we first introduce an antiunitary conjugation operation as

$$KJ_xK = J_x, KJ_yK = -J_y, KJ_zK = J_z, K^2 = 1, Kc|\psi\rangle = c^*|\psi\rangle^* \tag{4.7}$$

where c is any complex c-number. With the help of two unitary operators,

$$S = e^{ipJ_y} e^{i\pi J_z}, \quad \tilde{S} = e^{-i\pi J_x} e^{-ipJ_y}, \tag{4.8}$$

we define

$$T = SK, \quad \tilde{T} = \tilde{S}K. \tag{4.9}$$

These operators obey the useful identities

$$[K, S] = [K, \tilde{S}] = 0, \quad S^2 = \tilde{S}^2 = T^2 = \tilde{T}^2 = 1. \tag{4.10}$$

Moreover, T and $\tilde{T}$ are revealed as time reversal operations by

$$TUT = \tilde{T}U\tilde{T} = U^{-1}, \tag{4.11}$$

a relation identical in appearance with (3.8). It is also easily shown using (4.6–9) that

$$\begin{aligned} TJ_xT &= -J_x\cos p - J_z\sin p \\ TJ_yT &= J_y \\ TJ_zT &= -J_x\sin p + J_z\cos p. \end{aligned} \tag{4.12}$$

and

$$\begin{aligned} \tilde{T}J_x\tilde{T} &= J_x\cos p + J_z\sin p \\ \tilde{T}J_y\tilde{T} &= J_y \\ \tilde{T}J_z\tilde{T} &= J_x\sin p - J_z\cos p. \end{aligned} \tag{4.13}$$

Obviously, (4.12, 13) correspond to the classical transformations (3.4) and (3.5). Like the latter they are related to one another by the geometric symmetry R_y.

The consequences of time reversal invariance for the eigenvectors and eigenvalues of U are similar to the wellknown ones pertaining to time independent Hamiltonians. We shall discuss and use them in treating the statistics of the spacing of the eigenphases of U in Sect. 8.

5. Semiclassical Approximation

In studying the simplifications arising for large but finite values of j it is convenient to use the rescaled angular momentum operators

$$X_\pm = (J_x \pm iJ_y)/j, \quad Z = J_z/j \tag{5.1}$$

which obey $[X_+, X_-] = 2Z/j$, $[Z, X_\pm] = \pm X_\pm/j$. For $p=\pi/2$ the stroboscopic Heisenberg equations (2.3) then take the form

$$\begin{aligned} X'_+ &= e^{\frac{ik}{2j}}[Z + \tfrac{1}{2}(X_+ - X_-)]\, e^{-ik(X_+ + X_-)} \\ Z' &= -\tfrac{1}{2}(X_+ + X_-). \end{aligned} \tag{5.2}$$

We now assume a coherent initial state (2.6) and look for the expectation value of the X_i after n kicks,

$$\sigma_n \equiv \langle\gamma|\, U^{-n} X_+ U^n |\gamma\rangle$$
$$\zeta_n = \langle\gamma|\, U^{-n} Z U^n |\gamma\rangle. \tag{5.3}$$

As follows from (2.6, 7) the sequence (5.3) begins with

$$\sigma = 2\gamma/(1+\gamma\gamma^*)$$
$$\zeta = (1-\gamma\gamma^*)/(1+\gamma\gamma^*). \tag{5.4}$$

By using normal-ordering techniques and the commutation relations for the operators (5.1) it is easy to establish recursion relations for the expectation values (5.3) which generalize the classical map (3.1) by including first-order corrections with respect to $1/j$,

$$\begin{aligned}\sigma_{n+1} = {} & [\zeta_n + \tfrac{1}{2}(\sigma_n - \sigma_n^*)]\, e^{-ik(\sigma_n+\sigma_n^*)} \\ & + \tfrac{1}{2j} e^{-ik(\sigma_n+\sigma_n^*)} \{ik[\zeta_n + \tfrac{1}{2}(\sigma_n - \sigma_n^*)] \\ & + ik[D(\zeta_n, \sigma_n) + D(\zeta_n, \sigma_n^*) + \tfrac{1}{2} D(\sigma_n, \sigma_n) \\ & + \tfrac{1}{2} D(\sigma_n, \sigma_n^*) - \tfrac{1}{2} D(\sigma_n^*, \sigma_n) - \tfrac{1}{2} D(\sigma_n^*, \sigma_n^*)] \\ & - \frac{k^2}{2}[\zeta_n + \tfrac{1}{2}(\sigma_n - \sigma_n^*)][D(\sigma_n, \sigma_n) \\ & + D(\sigma_n, \sigma_n^*) + D(\sigma_n^*, \sigma_n) + D(\sigma_n^*, \sigma_n^*)]\}, \\ \zeta_{n+1} = {} & -\tfrac{1}{2}(\sigma_n + \sigma_n^*).\end{aligned} \tag{5.5}$$

It is, of course, due to the linearity of the second one of the operator recursion relations (5.2) that no $1/j$ correction shows up in the second one of the relation (5.5). The $1/j$ correction in σ_{n+1}, on the other hand, involves the following bilinear differential form,

$$\begin{aligned} D(A,B) = {} & -\sigma^2 \frac{\partial A}{\partial \sigma}\frac{\partial B}{\partial \sigma} - \sigma^{*2} \frac{\partial A}{\partial \sigma^*}\frac{\partial B}{\partial \sigma^*} - \sigma\sigma^* \frac{\partial A}{\partial \zeta}\frac{\partial B}{\partial \zeta} \\ & + (1+\zeta)^2 \frac{\partial A}{\partial \sigma}\frac{\partial B}{\partial \sigma^*} + (1-\zeta)^2 \frac{\partial A}{\partial \sigma^*}\frac{\partial B}{\partial \sigma} \\ & + (1-\zeta)\left[\sigma^* \frac{\partial A}{\partial \sigma^*}\frac{\partial B}{\partial \zeta} + \sigma \frac{\partial A}{\partial \zeta}\frac{\partial B}{\partial \sigma}\right] \\ & + (1+\zeta)\left[\sigma \frac{\partial A}{\partial \sigma}\frac{\partial B}{\partial \zeta} + \sigma^* \frac{\partial A}{\partial \zeta}\frac{\partial B}{\partial \sigma^*}\right] \end{aligned} \tag{5.6}$$

where A and B are functions of the initial expectation values σ, ζ and σ^*. Its formidable appearance notwithstanding the $1/j$ correction is not difficult to treat. Even though it represents a quantum effect we can work out its time dependence in zeroth order in $1/j$, i.e. by using classical dynamics; it thus behaves like an inhomogeneity in the first of the equations of motion (5.5).

The $1/j$ correction is bilinear in the elements of the matrix

$$M_n = \begin{pmatrix} \partial\sigma_n/\partial\sigma & \partial\sigma_n/\partial\zeta & \partial\sigma_n/\partial\sigma^* \\ \partial\zeta_n/\partial\sigma & \partial\zeta_n/\partial\zeta & \partial\zeta_n/\partial\sigma^* \\ \partial\sigma_n^*/\partial\sigma & \partial\sigma_n^*/\partial\zeta & \partial\sigma_n^*/\partial\sigma^* \end{pmatrix}. \tag{5.7}$$

We may use the chain rule of differentiation and represent the matrix M_n by a product of n matrices

$$M_n = \Delta_n \Delta_{n-1} \ldots \Delta_1 \tag{5.8}$$

where each factor Δ_l has the same structure as M_n itself except that σ_l, ζ_l, σ_l^* are differentiated with respect to σ_{l-1}, ζ_{l-1}, σ_{l-1}^*. In fact, Δ_l is nothing else than the classical map F written for spherical rather than cartesian components of the angular momentum vector and linearized around σ_{l-1}, ζ_{l-1}, σ_{l-1}^*. All of the matrices Δ_l as well as their product M_n thus have determinants equal to unity.

We must now distinguish two radically different situations. The first one arises when the kick strength k and the orientation $\{\theta, \phi\}$ of the initial state are chosen such that the classical map generates a chaotic trajectory; regular classical motion characterizes the second situation.

For the chaotic case, the very definition of Lyapounov exponents [19] entails that the three eigenvalues of M_n approach the exponential growth $e^{\lambda_i n}$ for large times. Due to angular momentum conservation one of the Lyapounov exponents must vanish, $\lambda_1 = 0$. The other two must have equal magnitude but different signs since our top has Hamiltonian dynamics, $\lambda_2 = -\lambda_3 \equiv \lambda > 0$. It follows that the $1/j$ correction in (5.5) behaves like external noise with an intensity growing exponentially in time. The $1/j$ expansion used in deriving the semiclassical equations of motion is thus invalidated after a time

$$n_{\text{chaos}} \sim (1/\lambda) \ln j. \tag{5.9}$$

Turning now to the case of regular classical motion we are facing a matrix M_n whose element at worst grow in time like some power n^α, $\alpha > 0$. Correspondingly larger is the domain of validity of the semiclassical approximation (5.5),

$$n < n_{\text{reg}} \sim j^{1/\alpha}. \tag{5.10}$$

In neither the regular nor the chaotic case can the semiclassical approximation (5.5) be used on the especially interesting time scale $n \sim j$ on which, as we shall see below, the quasiperiodicity of the quantum motion becomes manifest. An asymptotic long-time treatment would require a large-j approximation of U^j rather than of $U$and is not available at present.

6. Regular Versus Erratic Quasiperiodicity

The $2j+1$ eigenphases ϕ_ν of the unitary time evolution operator (2.2) can be thought of as lying in the interval $0 \leqslant \phi_\nu < 2\pi$. Their effective mean spacing is thus of the order π/j. Since the temporal resolution of a phase spacing $\Delta\phi$ requires times exceeding $1/\Delta\phi$

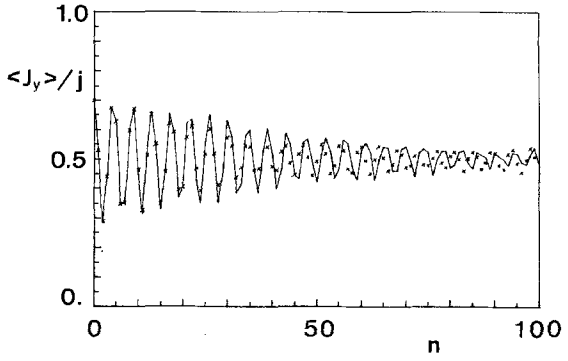

Fig. 2. Classical (crosses) and quantum (solid line) expectation value $\langle J_y \rangle_n$ for coherent initial state localized in classically regular region $\langle J_x \rangle_0 = -\langle J_z \rangle_0$, $\theta_y = 0.8$

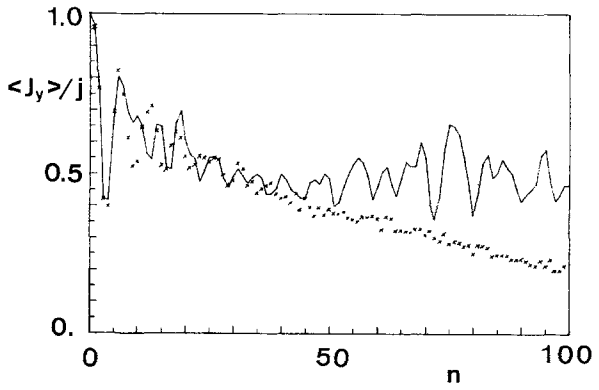

Fig. 4. As Fig. 2 but with coherent initial state localized in classically chaotic region at $\langle J_x \rangle_0 = -\langle J_z \rangle_0$, $\theta_y = 0.1$

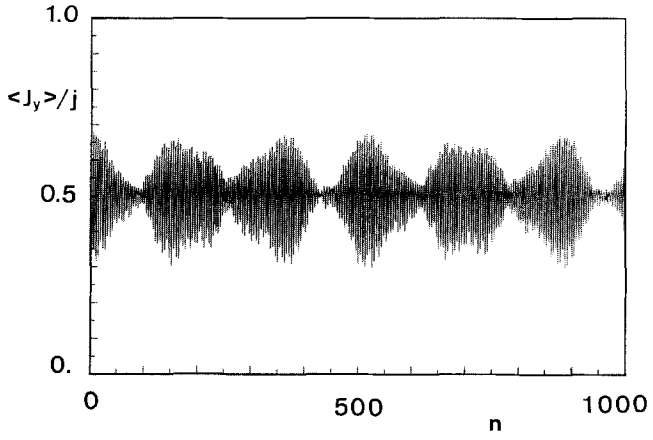

Fig. 3. Quantum mean as in Fig. 2 extended to large times to display the regular alternations of collapse and revivals

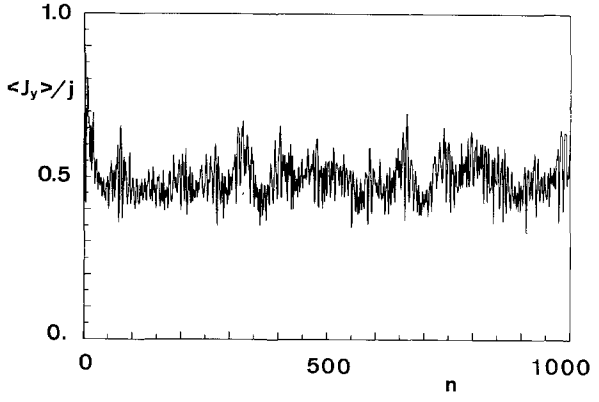

Fig. 5. Quantum mean as in Fig. 4 extended to large times to display the irregularity of recurrences

the quasiperiodicity of the quantum dynamics of our top becomes manifest for times of the order j. Classical chaos can therefore live in quantum expectation values as a transient only; it is definitely dead after a number of kicks of the order j.

Conversely, if we want to find out whether quantum chaos can be more than a mere transient mimicry of classical chaos we ought to study the quantum dynamics on a time scale of the order j, for large values of j. Such an investigation must be carried out numerically.

For the numerical calculation of time dependent expectation values we have employed two different strategies. One is to use the eigenstates $|jm\rangle$ of $\mathbf{J}^2$ and J_z to represent the operators U and $U^{-n} J_i U^n$ as $(2j+1)$ by $(2j+1)$ matrices. The alternative is to first diagonalize U and then spectrally synthesize time dependent expectation values by using the eigenvectors and eigenvalues of U. We have not been satisfied with our numerical results before both methods yielded agreement for $j=100$ and times up to $n \approx 1{,}000$.

In Figs. 2–5 we depict the time dependence of the expectation value of J_y for coherent initial states, $j=100$, and $k=3$. Figures 2 and 4 show the short-time behavior, $n \lesssim j$, and also contain classical ensemble averages $\langle Y \rangle$. The latter were evaluated from bundles of 1,000 classical trajectories originating from a cloud of initial points equal in location (θ, ϕ) and angular spread $(\sin\theta \Delta\theta \Delta\phi = 1/j)$ to the coherent state used in the quantum case.

For Fig. 2 we have chosen an initial state well within the classical stability island around the fixed point (3.15) with $X=-Z>0$, $Y>0$ (see Fig. 1c). The classical average (crosses) displays damped oscillations towards a stationary value $\langle Y \rangle_\infty \approx 0.5$. The oscillation corresponds to the classical orbiting of the regular trajectories around the stable fixed point; the oscillation period $\Delta n \approx 4$ compares favorably with the eigenvalues obtained by linearizing the map F around the fixed point. Actually, the nonlinearity of F attributes slightly different orbiting frequencies to the 1,000 trajectories in the classical ensemble. As the orbits gradually get out of phase with oneanother the classical average $\langle Y \rangle$ suffers a damping. The stationary value $\langle Y \rangle_\infty$ roughly equals the Y coordinate of

the classical fixed point. The quantum average $\langle J_y \rangle$ shows the same behavior qualitatively. There is even rather good quantitative agreement between the classical and the quantum averages during the first 10 or so oscillations; even for n up to $j=100$ the only difference between the two overages is in a slight phase shift. Such agreement is to be expected on the basis of the semiclassical analysis of Sect. 5, especially in view of (5.10).

For times exceeding j the quantum behavior is quite different from the classical one. While $\langle Y \rangle$ tends to a stationary value, if the number of points in the ensemble goes to infinity, the quantum average exhibits, as it must, quasiperiodicity. As shown in Fig. 3 the quasiperiodicity takes the form of a rather regular sequence of "collapses" and "revivals" [20]. The temporal separation of subsequent revivals, the quasiperiod, comes out as roughly 100 and that value nicely confirms the expectation based on the mean spacing $\Delta\phi \approx \pi/j$ of the eigenphases of U.

Figure 4 refers to an initial state localized within the classically chaotic region. In view of the semiclassical arguments presented in Sect. 5 it is not surprising to find significant differences between the classical and the quantum averages at rather early times, $n \approx 8$, already. Lateron, the classical average decays to zero. This decay signals a rather symmetric spread of the bundle of classical trajectories over the northern ($Y>0$) and southern ($Y<0$) hemispheres. Radically different is the quantum behavior for times $n>j$ (see Fig. 5). As in the regular case the quantum mean $\langle J_y \rangle$ keeps recurring to the neighborhood of its initial value [6, 21]. In striking contrast to the regular case the sequence of recurrences is seemingly erratic rather than having nearly equal spacings.

While the early-stage behavior of the quantum average in Figs. 4 and 5 can be interpreted as a reflection of classical chaos the erratic sequence of recurrences visible for times larger than j is a genuine quantum effect. It is quite interesting to see the quantum quasiperiodicity to manifest itself so drastically differently in Fig. 3 and Fig. 5. The difference certainly suggests that the distinction between regular and "chaotic" dynamics may not be an exclusive priviledge of classical mechanics.

In order to check whether the transition from orderly sequences of collapses and revivals to erratic recurrences can serve as at least a qualitative quantum criterion for chaos we have calculated the averages $\langle J_y \rangle_n$ for various coherent initial states. These states were chosen on the classical T line ($\langle J_x \rangle_0 = -\langle J_z \rangle_0$) with an angular separation $\theta_y = \langle (\hat{y}, \langle \mathbf{J}_0 \rangle$ from the precession axis ranging from 0.1 (as in Figs. 4 and 5, close to the hyperbolic fixed point at the pole $Y=1$.) to 1.1 (close to the classical elliptic fixed point with $X>0$), always keeping the kick strength $k=3$ and the precession angle $p=\pi/2$. Classically, the island of stability around the elliptic fixed point lies (see Fig. 1b) in the interval $0.6 \lesssim \theta_y \lesssim 1.4$; classical chaos prevails in $0 \leqslant \theta_y \lesssim 0.6$ while the intermediate range, $0.5 \lesssim \theta_y \lesssim 0.6$, accomodates both narrow chaotic bands and regular orbits. In the time dependence of the quantum average $\langle J_y \rangle_n$ we find clear regular modulations as in Figs. 2 and 3 for initial states with $1.1 \gtrsim \theta_y \lesssim 0.7$ but clearly erratic behavior like in Figs. 4 and 5 for $0.4 \gtrsim \theta \gtrsim 0.1$. The size of the intermediate region in which the transition from regular to erratic recurrences takes place is in harmony with the classical transition range and the angular width of the initial coherent states, $\Delta\theta_y = 1/\sqrt{j}$.

Needless to say that the qualitative difference between regular and erratic recurrences does not in itself constitute a "hard" criterion for quantum chaos. In searching such a criterion it might be interesting to study the width δn of the probability distribution of the temporal separations of recurrences of $\langle J_y \rangle$ to some close neighborhood of its initial value. The relative width $\delta n/j$ may behave quite differently at large j in the two cases. Evidently, more work is needed to explore such possibilities.

7. Quantum Beats Versus Broad-Band Excitation

Let us now turn to a spectral investigation of our quantum top based on the $2j+1$ eigenvectors and eigenvalues of U. We have found the number of eigenvectors necessary for a satisfactory synthesis of $\langle J_y \rangle_n$ to vary considerably when the initial coherent state is moved from a region of classically regular motion to one of classical chaos. For a quantitative discussion of this phenomenon we may employ the minimum number $N_{\min}$ of eigenvectors of Unecessary to exhaust the normalization of a coherent initial state to within, say, 1%. Figures 6a–c refer to coherent states on the classical T line and show $N_{\min}$ in its dependence on θ_y for $k=2$, 3 and 6. It is quite interesting to compare the θ_y dependence of $N_{\min}$ to that of the classical Lyapounov exponent which is also displayed in Fig. 6. Roughly speaking, $N_{\min}$ is large when the Lyapounov exponent is.

The two quantities appear correlated most interestingly for $k=3$. The rather flat minimum of $N_{\min}$, $N_{\min} \approx 8$, shows up close to the location of the classical elliptic fixed point, $\theta_y \approx 1.1$. As the neighboring chaotic regions are entered $N_{\min}$ grows by roughly an order of magnitude. The rather pronounced dips of $N_{\min}$ at the poles $\theta_y=0$ and $\theta_y=\pi$ are due to a symmetry. For coherent states living close to those poles only eigenvectors which are even under R_y for j even are

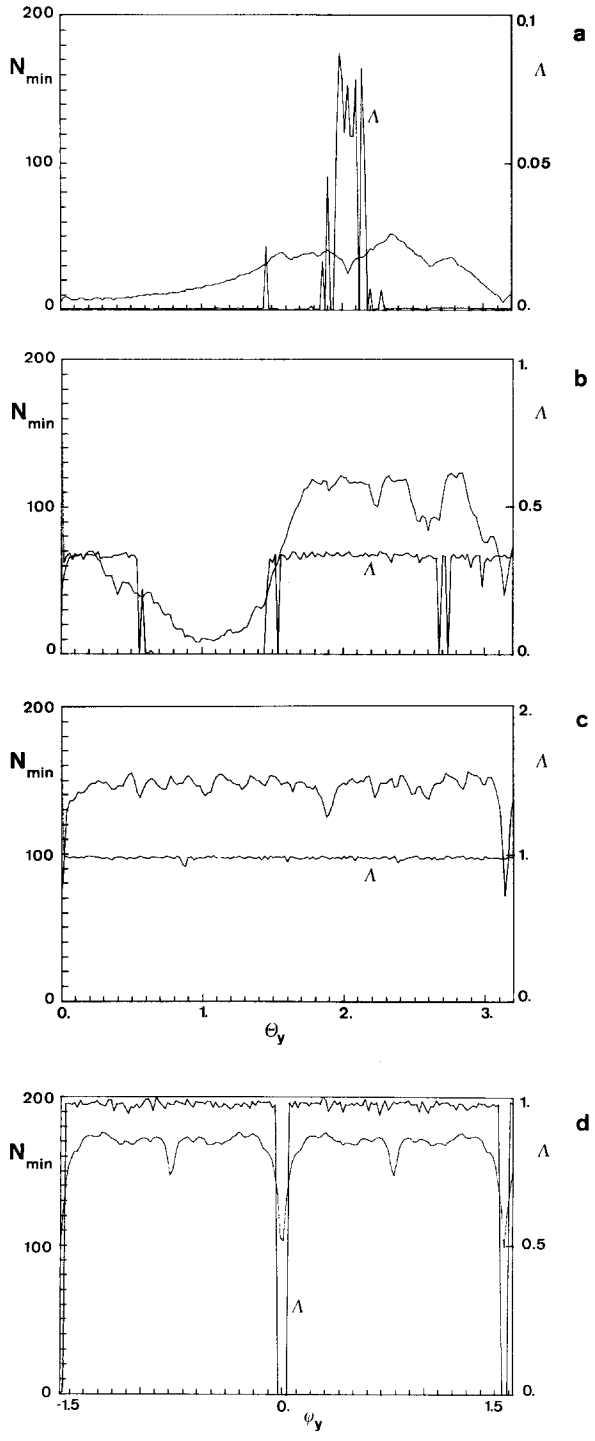

Fig. 6a–d. Minimal number of eigenstates $N_{\min}$ exhausting 99% of the normalization of the initial coherent state localized at θ_y, ϕ_y, and the corresponding largest Lyapounov exponent Λ. **a** on the classical T line $\left(\phi_y=-\frac{\pi}{4},\ 0\leqslant\theta_y\leqslant\pi\right)$, $p=\frac{\pi}{2}$, $k=2$; **b** on the classical T line $\left(\phi_y=-\frac{\pi}{4},\ 0\leqslant\theta_y\leqslant\pi\right)$, $p=\frac{\pi}{2}$, $k=3$; **c** on the classical T line $\left(\phi_y=-\frac{\pi}{4},\ 0\leqslant\theta_y\leqslant\pi\right)$, $p=\frac{\pi}{2}$, $k=6$; **d** on the equator $\left(\theta_y=\frac{\pi}{2},\ -\frac{\pi}{2}\leqslant\phi_y\leqslant\frac{\pi}{2}\right)$, $p=\frac{\pi}{2}$, $k=6$

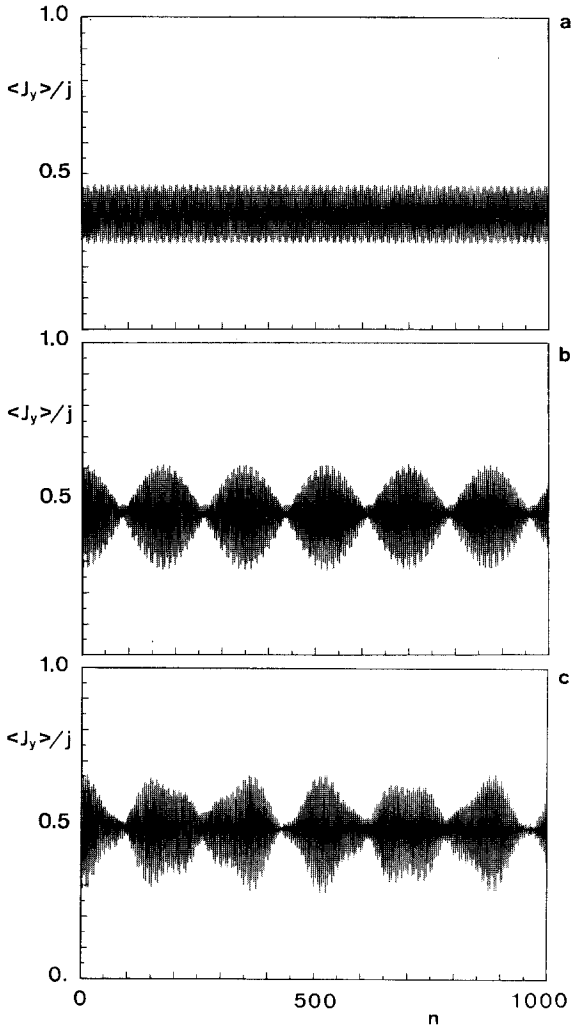

Fig. 7. Quantum mean $\langle J_y\rangle$ synthesized by the (a) four, (b) six, and (c) eight most important eigenvectors for $p=\frac{\pi}{2}$, $k=3$ and the initial state localized in classically regular region at $\langle J_x\rangle_0=-\langle J_z\rangle_0$, $\theta_y=0.8$. These results should be compared with Fig. 3

appreciably populated while everywhere else along the T line even and odd eigenvectors tend to show up in approximately equal numbers. Clearly, it is the priviledge of coherent states located close to the poles defined by the y axis not to be displaced much by rotations around that axis by π and thus to have very small components along the eigenvectors of U odd under R_y.

For $k=6$ our determination of the Lyapounov exponent does not reflect any regular motion anywhere along the T line. Correspondingly, $N_{\min}$ is large and rather uniform again except for the holes at the poles $\theta_y=0$, π. On the other hand the dips corresponding to 4-cycle (3.22) are clearly visible when we move along the equator $\left(\theta_y=\frac{\pi}{2}\right)$ rather than along T line (Fig. 6d).

The behavior of the Lyapounov exponent along the Tline for $k=2$ reveals a chaotic band $1.8 \lesssim \theta_y \leqslant 2.2$ around one point of the unstable 4-cycle (3.23) and a smaller such band close to $\theta_y \approx 1.5$ which pertains to the now unstable 6-cycle related to the pair of 3-cycles (3.24) by R_x. The variation of $N_{\min}$, on the other hand, is not sufficiently pronounced to yield a detailed correspondence to the classical behavior.

It is tempting to speculate that the correlation between the Lyapounov exponent and $N_{\min}$ grows stronger as the quantum number j is increased. It is certainly reasonable to expect $N_{\min}$ to scale as $\sqrt{j}$ for initial states well within the classically regular region since regular orbits are not qualitatively different from harmonic ones. Coherent initial states in the classically chaotic region should, on the other hand, pick up a fraction of the $2j+1$ eigenstates of U growing much faster with j, possibly with $N_{\min} \sim j$. If we could prove that conjecture we would have a quantum mechanical criterion for chaos complementary to the one suggested in the last section.

The relative smallness of $N_{\min}$ in regions of regular motion suggests an interpretation of the orderly sequence of collapses and revivals in Fig. 3 as a quantum beat phenomenon. This is made plain in Fig. 7a–c where $\langle J_y \rangle_n$ is synthesized by the four, six, and eight most important eigenvectors.

The erratic recurrences characteristic of chaotic motion now appear as due to the interference of a large number of eigenvectors, i.e. broadband excitation.

8. Level Repulsion

For kick strengths at which our top has regular classical trajectories over most of the sphere we can expect the eigenphases ϕ_n to have spacings with a Poisson distribution [10]. Figure 8 shows that expectation borne out nicely for $j=100$. Actually, to obtain a reasonably smooth level spacing distribution we had to superimpose the histograms pertaining to the 101 dimensional even subspace and the 100 dimensional odd subspace for five different kick strengths in the interval $0.1 \leqslant k \leqslant 0.3$ and $p=2$.

When we increase k to anywhere beyond 6 chaos dominates practically all of the classical sphere. The eigenphases ϕ_n must thus be expected to be equivalent in their statistical properties to the eigenvalues of "random" $(2j+1)$ by $(2j+1)$ matrices from an appropriate matrix ensemble. Among the ensembles which have been found to define different universality classes of level statistics we can confidently rule out the band-diagonal matrices whose eigenvectors show the effect

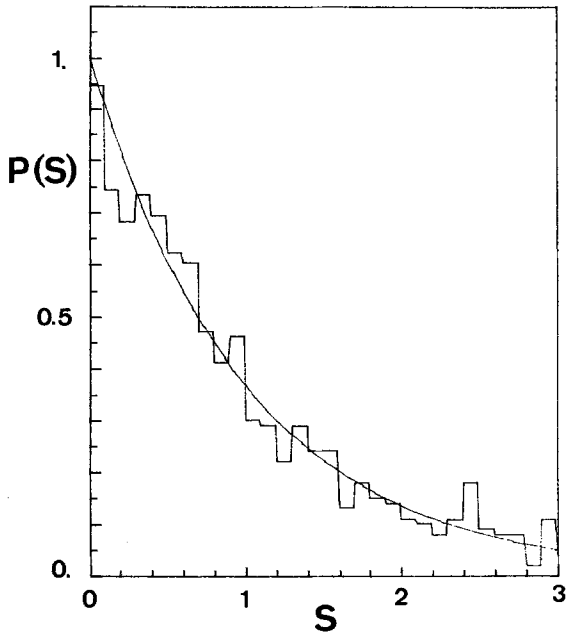

Fig. 8. Distribution of quasienergy spacings for the case when regular motion dominates classically, $p=2$, $0.1 \leqslant k \leqslant 0.3$. The smooth curve corresponds to the Poisson distribution $\exp(-S)$

of localization with respect to some "natural" representation [22]. If we represent our unitary operator U in the basis of eigenstates of any of the components of **J** we invariably find nonvanishing elements all over the matrix rather than a tendency of nonzero entries to cluster near the main diagonal. Typical eigenvectors of U should therefore not be "localized" with respect to any of these representations (provided k is set such one has global chaos classically). Speaking geometrically, typical eigenvectors will not have their supports on narrow solid angle ranges. This reasoning is also backed by the fact that the quantity $N_{\min}$ defined in the last section tends to be large everywhere on the sphere for the k values in question.

In order to investigate the statistics of our ϕ_n we shall now extend an argument originally given by Pechukas [23] (see also [24]) for autonomous Hamiltonian systems to periodically kicked ones. Let us consider time evolution operators of the general form

$$U(\lambda) = e^{i\lambda V} U_0, \quad V = V^+ \tag{8.1}$$

and inquire about the dependence of the eigenvectors $|\phi_n(\lambda)\rangle$ and the eigenvalues $\phi(\lambda)$ on the parameter λ (For our kicked top λ can be taken to be the kick strength k while $V = -J_z^2/2j$). The eigenvectors and eigenvalues pertaining to λ and $\lambda + \delta\lambda$ can be related to one another by lowest-order perturbation theory with respect to $V\delta\lambda$. As $\delta\lambda \to 0$ we obtain the following set of differential equations

$$\frac{\mathrm{d}}{\mathrm{d}\lambda}\phi_n = V_{nn}$$

$$\frac{\mathrm{d}}{\mathrm{d}\lambda}V_{nm} = \sum_{k(\neq n,m)} \mathrm{i}\,V_{nk}\,V_{km}\left\{\frac{1}{\mathrm{e}^{\mathrm{i}(\phi_n-\phi_k)}-1}-\frac{1}{\mathrm{e}^{-\mathrm{i}(\phi_m-\phi_k)}-1}\right\} + \mathrm{i}(1-\delta_{nm})\frac{V_{nm}(V_{mm}-V_{nn})}{\mathrm{e}^{\mathrm{i}(\phi_n-\phi_m)}-1}, \tag{8.2}$$

where

$$V_{nm} = \langle\phi_n(\lambda)\,|\,V\,|\,\phi_m(\lambda)\rangle.$$

We may interpret these differential equations as describing a flow in a phase space with ϕ_n and V_{nm} as generalized coordinates, and λ a "time". Alternatively, we may interpret them as showing how U moves about in a matrix ensemble the nature of which we want to find out. Having in mind that U tends to behave like a random matrix we assume the flow (8.2) to be ergodic. Instead of "time" averages over large λ intervals we can then employ ensemble averages to establish the statistics of the eigenvalues ϕ_n.

The phase space density $\rho(\{\phi_n\}, \{V_{nm}\}, \lambda\}$ must obey the continuity equation

$$0 = \frac{\partial}{\partial\lambda}\rho + \mathrm{Div}(\mathbf{V}_\rho) = \frac{\mathrm{d}}{\mathrm{d}\lambda}\rho(\{\phi_n(\lambda)\}, \{V_{nm}(\lambda)\}, \lambda) + \rho\,\mathrm{Div}\,\mathbf{V} \tag{8.3}$$

where the phase space divergence

$$\mathrm{Div}\,\mathbf{V} = \sum_n \frac{\partial\phi_{n'}}{\partial\phi_n} + \sum_{n,m}\frac{\partial V'_{nm}}{\partial V_{nm}} \tag{8.4}$$

is given by (8.2) as

$$\mathrm{Div}\,\mathbf{V} = \sum_{n\neq m}\mathrm{i}(\phi'_n-\phi'_m)/\{\mathrm{e}^{\mathrm{i}(\phi_m-\phi_n)}-1\} = -\frac{d}{d\lambda}\sum_{n\neq m}\ln|\mathrm{e}^{\mathrm{i}(\phi_n-\phi_m)}-1|. \tag{8.5}$$

The summation in (8.5) is over as many pairs n, m as there are independent real parameters in the set of off diagonal matrix elements V_{nm}. That number obviously depends of the dimension N of the Hilbert space the operators U and V live in (For our kicked top with even j we have $N=j+1$ and $N=j$ for the subspaces even and odd under R_y, respectively). If there is no restriction on V beyond Hermiticity, $V=V^+$, the number of independent pairs n, m is $N(N-1)$. Only half as many pairs are independent, however, if a generalized time reversal invariance holds as we shall show presently. Distinguishing the two cases by a parameter β which takes the values 1 and 2 for systems with and without such an invariance, respectively, we write the simplest solution of (8.3, 5) as

$$\rho \sim \prod_{n<m}|\mathrm{e}^{\mathrm{i}(\phi_n-\phi_m)}-1|^\beta. \tag{8.6}$$

If the flow (8.2) has no other constants of the "motion" the proportionality factor in (8.6) cannot depend on the phases ϕ_n and the matrix elements V_{nm} and is thus determined by normalization. The distribution ρ then yields the probability density of eigenphases in the ensemble of matrices within which $U(\lambda)$ moves ergodically. By suitably reducing [25] ρ we obtain the probability for two neighboring eigenphases to have the spacing S which reads, for $S\to 0$,

$$P(S)\,\mathrm{d}S \sim S^\beta. \tag{8.7}$$

Kicked systems thus display, as do autonomous Hamiltonian ones, linear or quadratic level repulsion depending on whether or not they possess a suitable time reversal invariance.

To verify the asserted consequence of time reversal invariance we represent the generalized time reversal as in (4.9)

$$T = SK,\quad TUT = U^+. \tag{8.8}$$

where K is an antiunitary conjugation operation and S a unitary operator. We assume T not to depend on λ and to obey (4.10). With respect to any antiunitary operator T obeying $T^2=1$ it is possible to transform any complete set of orthogonal vectors into another one with T invariant basis vectors [26], $T|\psi_k\rangle = |\psi_k\rangle$. In such a basis U is represented by a symmetric matrix since $U_{kl} = \langle K\psi_k|KU\psi_l\rangle^* = \langle T\psi_k|TU\psi_l\rangle^* = \langle\psi_k|\ TUT\ |\psi_l\rangle^* = \langle U\psi_k|\psi_l\rangle^* = U_{lk}$. Moreover, the eigenvectors $|\phi_n\rangle$ of U have real components ϕ_n^k along those $|\psi_k\rangle$ and are thus T invariant themselves,

$$T|\phi_n\rangle = |\phi_n\rangle. \tag{8.9}$$

To prove this [25] we decompose the matrix U_{kl} as $U=U_1+\mathrm{i}U_2$ with U_1 and U_2 both real and symmetric. The unitarity of U then yields $1=U^+U=U_1^2+U_2^2+\mathrm{i}[U_1, U_2]$ and thus $[U_1, U_2]=0$. As any pair of commuting real symmetric matrices U_1 and U_2 can be diagonalized simultaneously by a real orthogonal matrix R the columns of which contain the components ϕ_n^k of the common eigenvectors of U_1, U_2, and U. The T invariance (8.9) is an immediate consequence of the reality of the ϕ_n^k, $T\sum_k \phi_n^k\,|\psi_k\rangle = \sum_k \phi_n^k\,T|\psi_k\rangle = |\phi_n\rangle$.

We now differentiate in

$$T\mathrm{e}^{\mathrm{i}\lambda V}\,U_0\,T = U_0^+\,\mathrm{e}^{-\mathrm{i}\lambda V} \tag{8.10}$$

with respect to λ, set $\lambda=0$ and obtain the restriction imposed on the operator V by time reversal invariance,

$$TVT=U^{+}VU. \tag{8.11}$$

By taking matrix elements with respect to eigenstates of U we derive the symmetry

$$e^{-i\phi_n}V_{mn}=V_{nm}e^{-i\phi_m}. \tag{8.12}$$

This symmetry could also have been obtained as a conservation law for the flow (8.2). We have now shown time reversal invariance to effectively halve the number of independent offdiagonal elements of V and thus to imply linear level repulsion.

Further insight into the role of time reversal can be obtained from a perspective established by Dyson [25]. Dyson's "orthogonal" ensemble of unitary symmetric N by N matrices is defined by its invariance under any transformation $S\to\tilde{W}SW$ where W is an arbitrary unitary matrix and $\tilde{W}$ its transpose. Any member U of this ensemble can thus be represented with the help of a suitable unitary matrix A as

$$U=A\tilde{A},\quad A^{-1}=A^{+}. \tag{8.13}$$

Assume such a decomposition to hold for a U of the form (8.1) with a particular value of λ. To find the condition under which U remains within the orthogonal ensemble when λ is varied we consider an infinitesimally neighboring one

$$\begin{aligned}U(\lambda+\delta\lambda)&=U(\lambda)(1+iV\delta\lambda)=A\tilde{A}(1+iV\delta\lambda)\\&\equiv A(1+iM\delta\lambda)\tilde{A}.\end{aligned} \tag{8.14}$$

The last equation in (8.14) defines a matrix M as

$$M=\tilde{A}V\tilde{A}^{-1}. \tag{8.15}$$

Evidently, then, $U(\lambda+\delta\lambda)$ is symmetric if and only if M is. Choosing the eigenvectors $|\phi_n\rangle$ of $U(\lambda)$ as a basis we have

$$A=\tilde{A}=\sum_n e^{i\phi_n/2}|\phi_n\rangle\langle\phi_n|$$

and

$$M_{nm}=e^{i(\phi_n-\phi_m)/2}V_{nm}. \tag{8.16}$$

The symmetry of the matrix M, however, is just the identity (8.12) the compatibility of which with the evolution of $U(\lambda)$ in "time" is now obvious.

In order to compare the theoretically predicted level repulsion with numerical results for our top for $j=100$ we had to superimpose several level spacing histograms. Figure 9 is based on $10\times(101+100)$ eigenphases pertaining to ten different kick strengths in the interval $10.0\leqslant k\leqslant 10.5$ and $p=1.7$. We should note that we have chosen $p\neq\pi/2$ in order to avoid

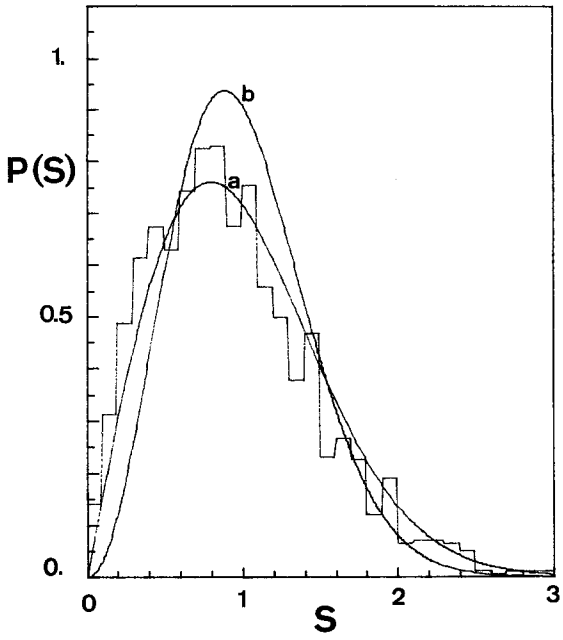

Fig. 9. Distribution of quasienergy spacings for the case when classically chaotic motion dominates; $p=1.7$, $10.0\leqslant k\leqslant 10.5$. The smooth curves correspond to (a) the Wigner distribution $\frac{1}{2}\pi S\exp\left(-\frac{\pi}{4}S^2\right)$ and (b) $\frac{32S^2}{\pi^2}\exp\left(-\frac{4}{\pi}S^2\right)$ which pertain to the cases of linear and quadratic repulsion, respectively

the symmetry (4.6) which would halve the number of independent ϕ_n in the odd subspace. Figure 9 quite convincingly reveals the expected linear level repulsion.

Let us finally turn to the most intriguing question as to how we have to modify the dynamics in order to achieve quadratic level repulsion [4, 9, 27]. As potential candidates we have studied the evolution operators

$$U(k',k,p)=e^{-i(k'/2j)J_x^2}e^{-i(k/2j)J_z^2}e^{-ipJ_y} \tag{8.17}$$

which differ from (2.2) by accounting for an additional nonlinear kick around the x axis. It is easy to see that in the special cases $p=\pi/2$ and $k'=k$ antiunitary generalized time reversal operators can again be constructed so that we must expect linear level repulsion. In the general case, however, we have not been able to identify any T invariance. Moreover, taking $U(0, k, p)$ as U_0 and $-J_x^2/2j$ as V in the sense of (8.1) we have verified that the flow (8.2) with $\lambda=k'$ is not compatible with the symmetry of the matrix (8.16). There is thus certainly no k' independent antiunitary operation T. While these findings do not prove that $U(k', k, p)$ typically lies within the so-called circular unitary ensemble we at least have no obvious reason to expect linear level repulsion. In fact, our numerical analysis for $j=100$, $p=1.7$, $\delta=0.5$ and the same set

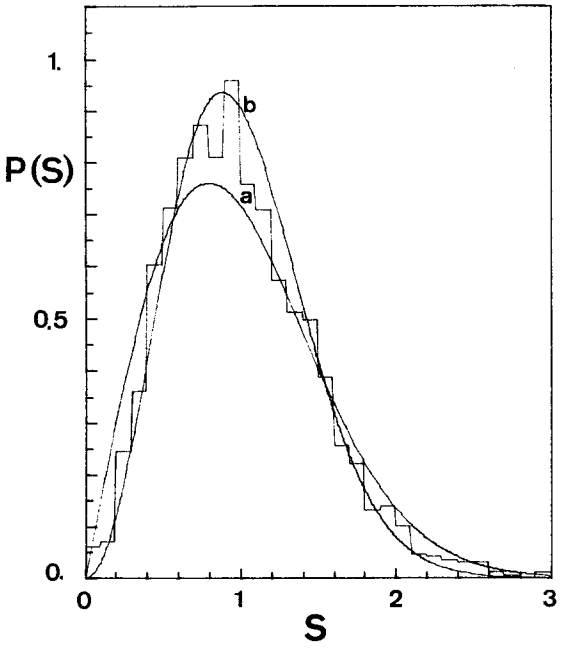

Fig. 10. Distribution of quasienergy spacings for the classically chaotic motion but with broken generalized time-reversal symmetry; $p=1.7$, $10.0 \leqslant k \leqslant 10.5$, $k'=0.5$. Smooth curves as in Fig. 9

of ten k values as in Fig. 9 suggests quadratic repulsion, as is shown in Fig. 10.

We gratefully acknowledge financial support of Marek Kuś by the Alexander von Humboldt-Stiftung and the Gesellschaft von Freunden und Förderern der Universität-Gesamthochschule Essen. We have benefitted from discussions with R. Graham, H. Frahm, S. Grossmann, H.J. Mikeska, S. Reynaud, and L. van Hemmen. During the early stages of this project we enjoyed the collaboration of J. Mostowski.

References

1. McDonald, S., Kaufman, A.N.: Phys. Rev. Lett. **42**, 1189 (1979)
2. Casati, G., Chirikov, B.V., Izrailev, F.M., Ford, J.: Stochastic behavior in classical and quantum hamiltonian systems. In: Lecture Notes in Physics. Casati, G., Ford, J. (eds.), Vol. 93, p. 334. Berlin, Heidelberg, New York: Springer 1979
3. Casati, G., Mantica, G., Guarneri, I.: In: Chaotic behavior in quantum systems. Casati, G. (ed.), p. 113. New York: Plenum Press 1985
4. Izrailev, F.M.: Quasi-energy level spacing distribution for quantum systems stochastic in the classical limit. (in Russian), Inst. of Nuclear Physics, Novosibirsk, Preprint No. 84–63 (1984)
5. Izrailev, F.M.: Phys. Rev. Lett. **56**, 541 (1986)
6. Hogg, T., Huberman, B.A.: Phys. Rev. Lett. **48**, 711 (1982)
7. Bohigas, O., Giannoni, M.J., Schmit, C.: Phys. Rev. Lett. **52**, 1 (1984)
8. Haller, E., Köppel, H., Cederbaum, L.S.: Phys. Rev. Lett. **52**, 1165 (1984)
9. Seligman, T.H., Verbaarscot, J.J.M.: Phys. Lett. **108A**, 183 (1985)
10. Berry, M.V., Tabor, M.: Proc. R. Soc. London Ser. A**356**, 375 (1977)
11. Haake, F., Kuś, M., Mostowski, J., Scharf, R.: In: Coherence, cooperation and fluctuations. Haake, F., Narducci, L., Walls, D. (eds.), p. 220. Cambridge: Cambridge University Press 1986
12. Frahm, H., Mikeska, H.J.: Z. Phys. B – Condensed Matter **60**, 117 (1985)
13. Arecchi, F.T., Courtens, E., Gilmore, R., Thomas, H.: Phys. Rev. A**6**, 2211 (1972)
14. Glauber, R.J., Haake, F.: Phys. Rev. A**13**, 357 (1976)
15. Waldner, F., Barberis, D.R., Yamazaki, H. Phys. Rev. A**31**, 420 (1985)
16. Reynaud, S.: Private Communication
17. McKay, R.S.: Renormalization in area preserving maps. Ph.D. thesis, Princeton 1982
18. DeVogelaere, R.: In: Contributions to the theory of nonlinear oscillations. Lefschetz, S. (ed.), Vol. IV, p. 53. Princeton: Princeton University Press 1958
19. Lichtenberg, A.J., Lieberman, M.A.: Regular and stochastic motion. Berlin, Heidelberg, New York: Springer 1982
20. Eberly, J.H., Narozhny, N.B., Sanchez-Mondragon, J.J.: Phys. Rev. Lett. **44**, 1323 (1980)
21. Graham, R., Höhnerbach, M.: in: Proceedings of the Topical Meeting on Instabilities and Dynamics of Lasers. Rochester 1985 (to be published)
22. Feingold, M., Fishman, S., Grempel, D.R., Prange, R.E.: Phys. Rev. B**31**, 6852 (1985)
23. Pechukas, P.: Phys. Rev. Lett. **51**, 943 (1983)
24. Yukawa, T.: Phys. Rev. Lett. **54**, 1883 (1985)
25. Dyson, F.J.: J. Math. Phys. **3**, 140, 157, 166 (1962)
26. Porter, C.E.: In: Statistical theories of spectra. Porter, C.E. (ed.), p. 3. New York: Academic Press 1965
27. Robnik, M., Berry, M.V.: J. Phys. A**19**, 669 (1986)

F. Haake
R. Scharf
Fachbereich Physik
Universität –
Gesamthochschule Essen
Postfach 103764
D-4300 Essen 1
Federal Republic of Germany

M. Kuś
Institute of Theoretical Physics
Warsaw University
Hoza 69
PL-00-681 Warsaw
Poland